Geophysical Research Letters

RESEARCH LETTER
10.1029/2019GL082943

Key Points:
- Relationship between WWV and Niño3.4 SST varies on decadal timescales, corresponding to the occurrence frequency of central Pacific ENSO
- Both eastern and central Pacific ENSO events show recharge/discharge signatures but with different WWV/Niño3.4 phase-lag relationships
- This difference can be explained by the existence of two different ENSO types characterized by distinct intrinsic periodicities

Supporting Information:
- Supporting Information S1

Correspondence to:
W. Zhang,
zhangwj@nuist.edu.cn

Citation:
Zhang, W., Li, S., Jin, F.-F., Xie, R., Liu, C., Stuecker, M. F., & Xue, A. (2019). ENSO regime changes responsible for decadal phase relationship variations between ENSO sea surface temperature and warm water volume. *Geophysical Research Letters*, *46*, 7546–7553. https://doi.org/10.1029/2019GL082943

Received 22 MAR 2019
Accepted 12 JUN 2019
Accepted article online 20 JUN 2019
Published online 1 JUL 2019

ENSO Regime Changes Responsible for Decadal Phase Relationship Variations Between ENSO Sea Surface Temperature and Warm Water Volume

Wenjun Zhang[1], Sixu Li[1], Fei-Fei Jin[2], Ruihuang Xie[3], Chao Liu[1], Malte F. Stuecker[4,5], and Aoyun Xue[1]

[1]CIC-FEMD/ILCEC, Key Laboratory of Meteorological Disaster of Ministry of Education (KLME), Nanjing University of Information Science and Technology, Nanjing, China, [2]Department of Atmospheric Sciences, SOEST, University of Hawai'i at Mānoa, Honolulu, HI, USA, [3]CAS Key Laboratory of Ocean Circulation and Waves, Institute of Oceanology, Chinese Academy of Sciences, Qingdao, China, [4]Center for Climate Physics, Institute for Basic Science, Busan, South Korea, [5]Pusan National University, Busan, South Korea

Abstract The relationship between the equatorial Pacific warm water volume (WWV) and El Niño–Southern Oscillation (ENSO) sea surface temperature (SST) has varied considerably on decadal timescales. These changes are strongly related to the occurrence frequency of central Pacific (CP) ENSO events. While both eastern Pacific (EP) and CP ENSO events show clear signatures of WWV recharge/discharge, their phase-lag relationships between WWV and Niño3.4 SST are different. The WWV usually leads the Niño3.4 SST by two to three seasons during EP ENSO, while the lead time is reduced to one season during CP ENSO. The different phase-lag relationships can be explained by distinct periodicities of the two ENSO types. Hence, ENSO regime changes associated with decadal predominance of either EP or CP ENSO events can give rise to decadal variations in the statistical WWV-ENSO SST relationship. We emphasize the importance of identifying these different ENSO types and potentially different ENSO regimes to assess ENSO predictability.

1. Introduction

The El Niño–Southern Oscillation (ENSO) is a phenomenon of fluctuations between warmer (El Niño) and colder (La Niña) sea surface temperature (SST) conditions in the eastern equatorial Pacific and associated coupled changes in the atmospheric circulation, which causes pronounced climate anomalies around the globe (McPhaden et al., 2006; Timmermann et al., 2018; Wallace et al., 1998). As the primary source of year-to-year climate variability, ENSO owes its existence to large-scale coupled ocean-atmospheric interactions in the equatorial Pacific (e.g., Bjerknes, 1969; Cane & Zebiak, 1985; Neelin et al., 1998; Wyrtki, 1975). Individual events can be predicted up to three seasons in advance due to the slow equatorial heat content recharge/discharge in the upper ocean (Cane & Zebiak, 1985; Wyrtki, 1985; Zebiak, 1989). The recharge/discharge oscillator theory captures ENSO's fundamental oscillatory behavior by describing interaction between SST and the slow ocean adjustment to the anomalous atmospheric circulation (Jin, 1997). This theory has been substantiated by long-term observations of the equatorial thermocline depth evolution and its relationship to eastern equatorial SST (Meinen & McPhaden, 2000). It considers both fast processes (i.e., the Bjerknes positive feedback) and the slow ocean adjustment dynamics arising from the disequilibrium between zonal winds and warm water volume (WWV; volume of water above 20 °C isotherm in the equatorial Pacific 5°S to 5°N, 120°E to 80°W). The WWV, describing upper Pacific Ocean heat content, usually leads the ENSO SST evolution by a quarter of the ENSO period (approximately two to three seasons) and acts as a useful predictor for ENSO SST (McPhaden, 2003). The recharge-discharge dynamics involve both thermocline shoaling (deepening) and easterly (westerly) geostrophic zonal current, corresponding to the thermocline and zonal advective feedbacks, respectively (Ren & Jin, 2013). Recent studies argued that the WWV in the western equatorial Pacific could be a better ENSO predictor beyond 1-year lead (Izumo et al., 2019; Planton et al., 2018).

However, this phase-lag relationship between the WWV and ENSO SST has experienced a significant shift around 2000 with the lead time being shortened from approximately two to three to approximately one seasons (Bosc & Delcroix, 2008; Bunge & Clarke, 2014; Horii et al., 2012; McPhaden, 2012; Neske & McGregor,

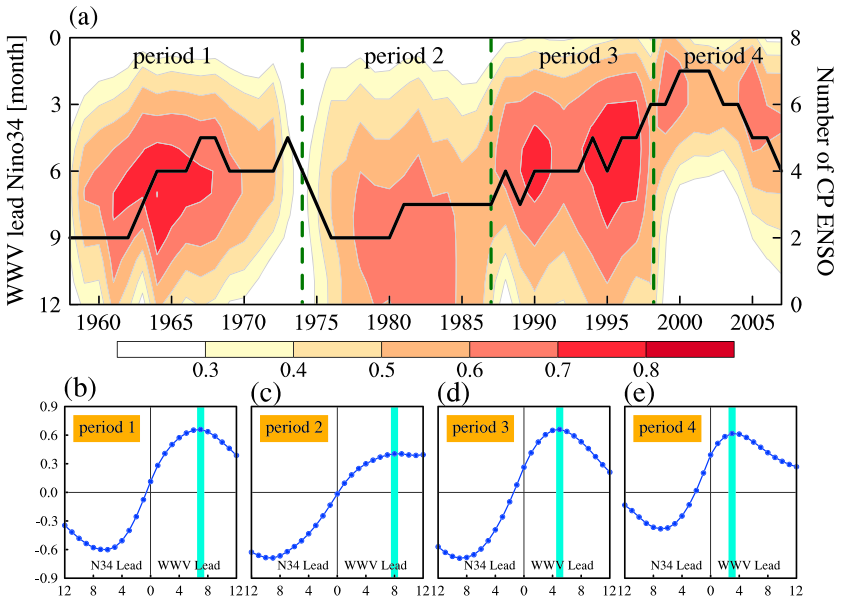

Figure 1. (a) Correlation (shading) between the warm water volume (WWV) and Niño3.4 indices as a function of WWV lead month (left *y* axis) and year (*x* axis), overlaid by the number of central-Pacific (CP) El Niño–Southern Oscillation (ENSO) events (right *y* axis), both within a 11-year running window (black thick line). Year in the *x* axis of (a) denotes the starting year of each 11-year window. (b–e) Cross correlation between the WWV and Niño3.4 indices during four periods (b) 1958–1974, (c) 1975–1987, (d) 1988–1998, and (e) 1999–2016, which are separated by green dashed lines in (a). The aquamarine bars indicate the lead months when the lead-lag correlation coefficients of WWV and Niño3.4 index attain their maximum value.

2018). Also, operational ENSO predictability in the recent two decades declined to an effective lead time of only one season, much shorter than the average predictability before 2000 (Hendon et al., 2009; Wang et al., 2010). It is compelling to link the shorter WWV-ENSO SST lead time and reduced ENSO predictability, since the upper ocean heat content provides the ocean memory for the long-lead predictability of ENSO. The decadal change of the WWV-ENSO SST phase-lag relation around 2000 was also accompanied by more frequent occurrences of central Pacific (CP) El Niño events, which are characterized by an air-sea action center that is shifted to the CP compared to traditional El Niño events with maximum SST anomalies in the eastern Pacific (EP; Ashok et al., 2007; Kao & Yu, 2009; Kug et al., 2009; Ren & Jin, 2011). It is speculated that the WWV and ENSO SST phase-lag relation change is possibly associated with this occurrence of more frequent CP El Niño events and a potential reduction in the effectiveness of the thermocline feedbacks (Horii et al., 2012; McPhaden, 2012). However, a different study argued that the thermocline feedback also plays a considerable role in the growth and phase transition of CP El Niño events, similar to EP El Niño events (Ren & Jin, 2013).

Actually, the WWV-ENSO SST relationship varies on decadal timescales since the middle 1950s (Bunge & Clarke, 2014; also see Figure 1a), which provides a larger sample size to investigate the associated mechanisms. The decades with reduced lead time are argued to be characterized by a westward displacement of zonal wind forcing associated with a La Niña-like tropical Pacific mean state. This decadal change is well observed after 2000 but seems obscure before the early 1970s (see Figure 8 in Bunge & Clarke, 2014). The WWV-ENSO SST phase-lag relationship and their decadal changes are worthy of further attention to deepen our understanding of potential ENSO predictability. In particular, it is still unclear what the dynamical linkages between WWV and ENSO SST are for different El Niño flavors and whether the El Niño regime shift contributes to the decadal variations of the WWV-ENSO SST relationship. In addition, La Niña events should also be separated into two types based on their different coupled air-sea dynamics and climate impacts (Shinoda et al., 2011; Zhang et al., 2015). Whether the relative occurrence frequency of the La Niña types contributes to the varying WWV-ENSO SST relationship is also unknown. In this paper, we demonstrate that the decadal variations of the WWV-ENSO SST relationship are predominantly governed by the relative EP/CP ENSO (both El Niño and La Niña) occurrence frequencies in different decades.

2. Data and Methodology

ENSO associated SST anomalies (SSTA) were derived based on the Extended Reconstructed Sea Surface Temperature, version 5 from the National Oceanic and Atmospheric Administration (Huang et al., 2017). The associated subsurface ocean temperatures were investigated using the ECMWF Ocean Reanalysis System product (Balmaseda et al., 2013). The WWV is defined as the volume of water integrated above 20 °C isotherm in the equatorial Pacific 5°S to 5°N, 120°E to 80°W (Meinen & McPhaden, 2000). Anomalies were calculated as the departures from the climatological monthly mean in the entire study period (1958–2017) and were linearly detrended to remove the possible influences from the long-term trend. The nondetrended data are also examined and the results are almost the same. Statistical significance was determined based on the two-tailed Student's *t* test.

We utilize the Climate Prediction Center definition to identify ENSO events based on a threshold of ±0.5 °C of the Niño3.4 index (averaged SSTA in the domain of 5°S to 5°N, 90° to 150°W) for five consecutive overlapping months. We further classify these ENSO events into two types (Table S1 in the supporting information) based on the analysis of their SSTA spatial structure, following our previous studies (Zhang et al., 2014, 2015). Here, ENSO events are classified as EP if the maximum SSTA (averaged over 5°S to 5°N) are located east of 150°W during the ENSO developing and mature phase and CP if the maximum SSTA are located west of this longitude. This method can well distinguish SSTA patterns associated with the two ENSO types (Figure S1). The EP and CP ENSO indices (EPI and CPI) were also calculated based on a simple rotation of the commonly used Niño3 (averaged SSTA in the domain of 5°S to 5°N, 90° to 150°W) and Niño4 (averaged SSTA in the domain of 5°S to 5°N, 160°E to 150°W) indices (Ren & Jin, 2011).

A modified version of the Zebiak-Cane (MZC) coupled intermediate complexity model (Xie & Jin, 2018) is used to further examine the WWV-Niño3.4 SST phase-lag relation. Model improvements are mainly conducted in the atmospheric component, such as introducing a heating efficiency factor related to the SST and wind convergence state and considering the effect of the convective momentum transport which jointly improve the simulated ENSO wind responses. The MZC has a certain ability to illustrate the air-sea interactions associated with EP and CP ENSO-like oscillatory modes (Figure S2). According to Xie and Jin (2018), the linear unstable EP and CP ENSO-like modes coexist under most climate conditions. In the nonlinear simulations, these two leading modes can be both excited with finite amplitudes. They can also be modified by nonlinearity and interact nonlinearly as well. This causes nonlinear bimodal interaction and irregular alternations of EP and CP ENSO events in nonlinear simulations. To obtain ENSO regimes where one type of ENSO dominates, two model experiments are designed to make only one ENSO mode unstable while the other mode is heavily damped in the linear eigen-analysis. In each of these regimes, either the EP or CP ENSO type is the major type in the nonlinear simulation (see experiment design in the supporting information). Both linear eigen analysis results and nonlinear simulations are used to highlight the different WWV-Niño3.4 SST phase-lag relations for the two types of ENSO under different ENSO regimes. The thermocline depth anomaly is averaged between 5°S and 5°N, used as a proxy of WWV for the model simulations.

3. Results

We first investigate the phase-lag relationships between the WWV and the Niño3.4 index (Figure 1). We find that their relationship exhibits pronounced decadal variability. The entire period (1958–2017) can roughly be separated into four periods, for which the lead times of the WWV over Niño3.4 change. In the second period (period 2: 1975–1987), the WWV leads Niño3.4 by approximately three seasons with a correlation of ~0.5 (Figure 1a and 1c). The lead time is reduced to approximately two seasons in the first (period 1: 1958–1974) and third (period 3: 1988–1998) periods with the highest correlation coefficients attaining values as high as 0.7 (Figures 1a, 1b, and 1d). In the fourth period (period 4: 1999–2017), the lead time is further reduced to only approximately one season (Figures 1a and 1e). As mentioned earlier, the shift of the WWV-Niño3.4 phase-lag relation around 2000 has been reported in previous studies (Bunge & Clarke, 2014; Horii et al., 2012; McPhaden, 2012). Interestingly, the number of CP ENSO (El Niño and La Niña) occurrences (black thick line in Figure 1a) corresponds well to the decadal variations for the WWV-Niño3.4 phase-lag relationship. To detect which type of ENSO is dominant in these different periods, we calculate the proportions of the number of CP ENSO events relative to the number of EP ENSO events. The

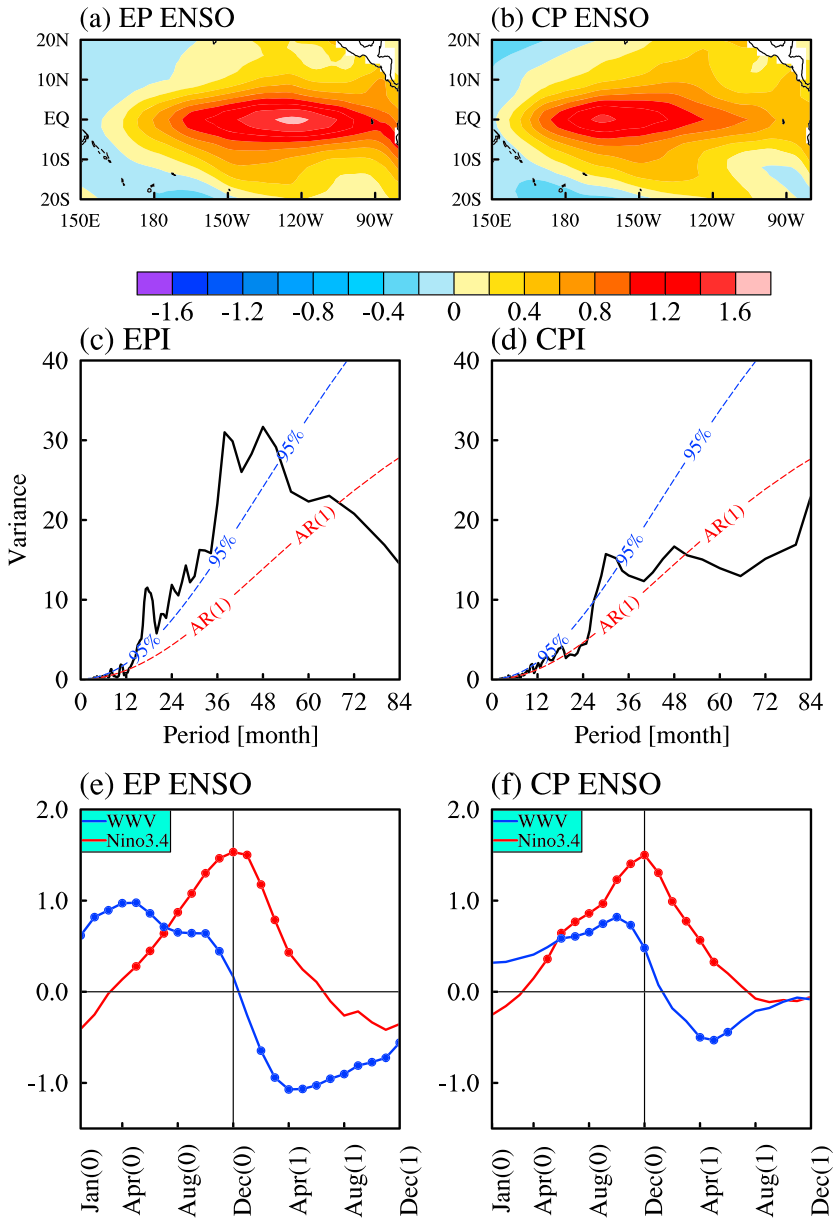

Figure 2. Composite December–February-mean SST anomaly patterns (°C) for (a) eastern Pacific (EP) and (b) central Pacific (CP) El Niño–Southern Oscillation (ENSO) events (0.5*[warm minus cold phase]). Fast Fourier transform power spectrum for the (c) EPI and (d) CPI indices (black thick line). Red and blue dashed lines correspond to an AR(1) null hypothesis and 95% confidence level, respectively. Composite evolution of the normalized warm water volume (WWV; blue line) and Niño3.4 indices (red line) for (e) EP and (f) CP ENSO events. Markers indicate the values that are statistically significant at the 90% confidence level.

proportions are 1.0 (3 CP/3 EP), 0.75 (3 CP/4 EP), 2.0 (4 CP/2 EP), and 3.0 (6 CP/2 EP), respectively, for these four periods. This suggests that the decadal changes in the WWV-Niño3.4 relationship could be related to different ENSO regimes associated with relative predominance of either EP or CP ENSO (both El Niño and La Niña) events.

We next examine the distinctive temporal and spatial features of the two ENSO types by emphasizing the El Niño-minus-La Niña composites of the same type (i.e., EP or CP). The two ENSO types are characterized by very different zonal SSTA structures with centers approximately at 125°W and 165°W for EP and CP types, respectively (Figures 2a and 2b). Correspondingly, distinct ENSO periodicities are seen for the two ENSO

types according to the power spectra of the EPI and CPI (Figures 2c and 2d). These two indices can roughly capture the temporal features of ENSO although they (and other current indices available) do better in identifying two distinct El Niño types but perform not well in separating distinct La Niña types (Zhang et al., 2015). It can be seen that the EP ENSO index is dominated by power at ~3- to 4-year periodicities, whereas the CP ENSO index displays a major peak at ~2–3 years. These observed periodicities are consistent with those of the theoretical unstable quasi-quadrennial and quasi-biennial ENSO modes in the Zebiak-Cane model (Bejarano & Jin, 2008; Xie & Jin, 2018).

Whether these two ENSO types exhibit different recharge-discharge processes is further examined. As shown in Figures 2e and 2f, the two ENSO types exhibit very similar seasonal SSTA evolutions as they both initiate in the early boreal summer, reach their peak in boreal winter, and decay in the following boreal spring. In contrast, their associated WWVs evolve differently. For the EP ENSO, the preceding positive WWV (the recharge process) is evident more than one year in advance compared to the Niño3.4 SSTA. The WWV reaches its maximum during ENSO developing spring months with an 8-month lead, consistent with the classic recharge-discharge theory (Jin, 1997). Then the WWV decreases and enters the discharge process during the EP ENSO peak phase in boreal winter. A similar WWV evolution is seen for CP ENSO, but with a much faster timescale. Significantly positive WWV is observed in the summer of the CP ENSO developing year and reaches its peak value during autumn, showing a one-season lead time over the Niño3.4 index. Almost the same evolutions of the WWV and Niño3.4 index are obtained for the EP and CP ENSO based only on data since 1980, when the subsurface ocean data quality improved considerably (Figure S3). This composite result indicates clearly that the recharge-discharge mechanism is operating in the ENSO cycle for both types, but with significantly different lead time. The difference of the WWV-Niño3.4 phase-lag relationship is also evident in separate El Niño and La Niña composites (Figure S4). Both El Niño and La Niña events show almost the same evolution as in the El Niño-minus-La Niña composites, suggesting that the WWV-Niño3.4 phase-lag relation depends on different ENSO types and not crucially dependent on ENSO warm or cold phases. These results also provide dynamic evidence for the necessity to classify ENSO into different types, both for El Niño and La Niña. Previous theoretical studies argued that a westward shift of the ENSO-related air-sea action center would give oceanic waves less time until they are reflected at the Pacific western boundary, which would induce a faster ocean adjustment (Clark, 2010; Fedorov, 2010). Hence, the WWV evolution tends to be more in phase with the zonal tilt mode as measured by Niño3.4 SSTA.

In the observations, both EP and CP ENSO modes usually coexist, which causes a certain degree of difficulty to extract the pure dynamics associated with each type. Thus, we employ the MZC model to illustrate the different recharge-discharge dynamics associated with the two ENSO types, since this new version of the model can generate different ENSO types well under different climate mean states (Xie & Jin, 2018). In the linear eigen analysis under a mean state that is similar to the present climate, the EP and CP ENSO-like modes are the only two unstable modes (Figures 3a and 3b), and their periodicities are distinct with a quasi-4-year period for the EP mode and a quasi-2-year period for the CP mode (Figures 3c and 3d). The simulated ENSO spatiotemporal features closely resemble the observations. The lower frequency seen in the observed CP ENSO index is possibly associated with a partial inclusion of the EP ENSO signal in the CPI because of its limitation in distinguishing two types of La Niña. We emphasize that model biases and simplifications might also contribute to this difference since some physical processes are missing in this intermediate complexity model.

Importantly, the recharge-discharge dynamics are clearly evident in both EP and CP ENSO-like modes in the model (Figures 3e and 3f). As in the observations, they exhibit different lead times of the WWV over the Niño3.4 index. The WWV leads the Niño3.4 by ~12 months for the EP mode and ~6 months for the CP mode, respectively, corresponding to one fourth of the respective ENSO mode periodicities. Therefore, the WWV-Niño3.4 relationships are consistent with the recharge-discharge theory (Jin, 1997) for both types of ENSO. Since both ENSO types are regulated by recharge-discharge dynamics but exhibit different intrinsic periodicities, it is easily expected that the lead time of the WWV over Niño3.4 is shorter for CP ENSO compared to EP ENSO. We emphasize that the simulated WWV lead time is larger than that seen in the observations, possibly due to presence of noise and ENSO-neutral conditions in the observations. To examine possible effects of nonlinearities, we conduct nonlinear simulations of the MZC model (see details in section 2 and the supporting information) and EP and CP ENSO regimes are examined separately. Our

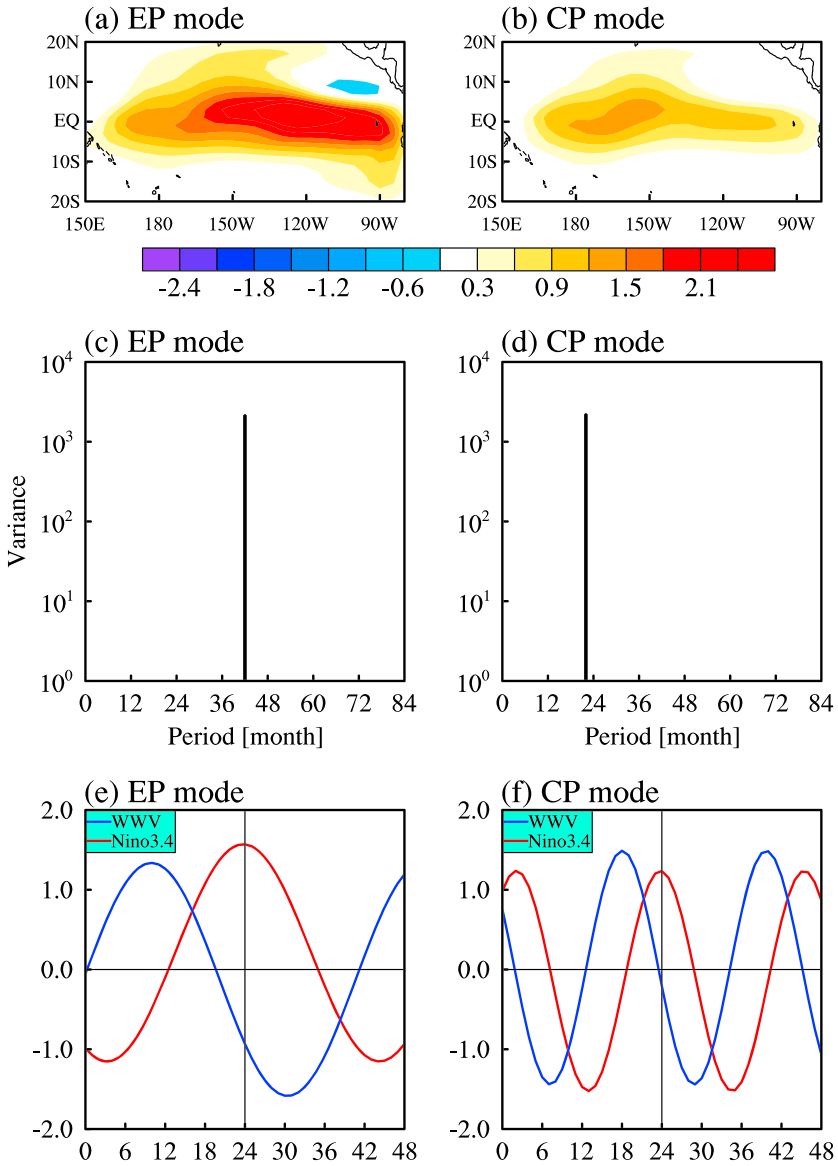

Figure 3. (a) Spatial sea surface temperature anomaly pattern, (c) fast Fourier transform power spectrum and (e) a 4-year evolution of the normalized warm water volume (WWV; blue line) and Niño3.4 indices (red line) for the eastern Pacific (EP) El Niño–Southern Oscillation (ENSO) mode extracted from the linearized MZC model. (b), (d) and (f) are the same as (a), (c), and (e) but for the central Pacific (CP) ENSO mode.

conclusions remain the same, with the characteristics in the nonlinear simulations looking closer to the observations for the periodicity (Figure S5). The modeling results of the MZC model also suggest that the background state changes are one potential source for different ENSO types, as shown in the previous studies (Bejarano & Jin, 2008; Xie & Jin, 2018).

Our analysis demonstrates that recharge-discharge processes occur in both EP and CP ENSO and that the lead time of WWV compared to Niño3.4 are determined by their distinct periodicities. WWV usually leads Niño3.4 by approximately three seasons for EP ENSO and by approximately one season for CP ENSO, respectively. Therefore, the WWV-Niño3.4 phase-lag relationship is closely related to the occurrence frequencies of each ENSO types in different decadal windows. For example, the much more frequent occurrence of CP ENSO events after 2000 explains the shorter WWV lead time compared to the preceding period (1988–1998; Figure 1a).

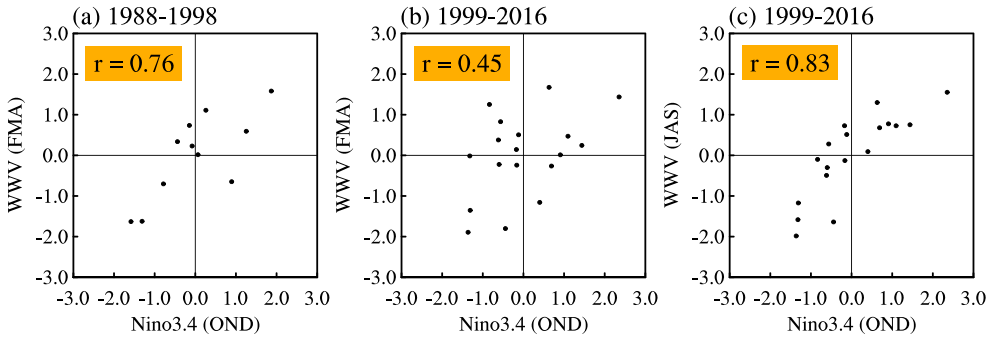

Figure 4. Scatter plots of normalized (a) February–March (FMA)-mean warm water volume (WWV) during period 3 in Figure 1, (b) FMA-mean WWV during period 4, and (c) January–September (JAS)-mean WWV during period 4 as a function of the normalized October–December (OND)-mean Niño3.4 index. Linear correlations are also shown in the inserts.

4. Discussion

In recent decades, the upper ocean heat content (measured by the WWV) displayed a remarkable shift in its lead-lag relation with ENSO SSTA (measured by the Niño3.4 index). Analyses of longer data records show that this shift around 2000 is one example of prominent decadal variations in the WWV-Niño3.4 phase-lag relationship, which can be attributed to decadal ENSO regime shifts. Different regimes are characterized by the predominance of either EP or CP ENSO in different decades. Despite the occurrence of different ENSO regimes, we find that oceanic recharge-discharge dynamics play important roles in both EP and CP ENSO events but with different periodicities. WWV usually leads Niño3.4 SSTA by approximately two to three seasons for both EP El Niño and La Niña events, whereas the lead time is reduced to approximately one season for both CP El Niño and La Niña events. Therefore, in decades with more frequent occurrences of CP ENSO events, the lead time of WWV over Niño3.4 decreases.

One previous study argued that the conventional WWV-Niño3.4 relationship did not hold in recent decades (Horii et al., 2012), which would cause difficulties for future ENSO predictions. Here we show that the ocean memory associated with heat content recharge-discharge still co-occurs with the ENSO evolution during these decades and that WWV still acts as an ENSO precursor but with significantly reduced lead time. Taking the period of 1999–2016 as an example, the boreal summer WWV still exhibits a relatively high correlation with the following winter Niño3.4 index (Figure 4a), although the linkage between spring WWV and winter Niño3.4 is weak and statistically insignificant (Figure 4b). Therefore, the WWV-ENSO SSTA relationship is crucially dependent on ENSO regimes associated with EP and CP types. However, current dynamical and statistical ENSO forecast models have difficulties in simulating two distinct ENSO types, thus potentially explaining decreases in forecast skill in decades that were characterized by frequent occurrences of CP ENSO events. Moreover, the shorter WWV lead time for CP ENSO events also potentially contributes to a reduction in forecast skill (Hendon et al., 2009; Wang et al., 2010). Finally, CP ENSO events are typically characterized by smaller SSTA amplitude compared to EP ENSO events. Hence, the signal-to-noise ratio is reduced for CP ENSO events, which could also contribute to the observed reduction in forecast skill for this type of events.

Acknowledgments
The data used to reproduce the results of this paper are located at https://www.esrl.noaa.gov/psd/data/gridded/data.noaa.ersst.v5.html and https://www.ecmwf.int/en/research/climate-reanalysis/ocean-reanalysis. This work was supported by the National Key Research and Development Program (2018YFC1506002), the SOA Program on Global Change and Air-Sea interactions (GASI-IPOVAI-03), and the National Nature Science Foundation of China (41675073 and 41506017). F.-F. Jin was supported by the U.S. National Science Foundation grant AGS-1406601 and the U.S. Department of Energy grant DE-SC000511. M. F. Stuecker was supported by the Institute for Basic Science (project code IBS-R028-D1).

References

Ashok, K., Behera, S. K., Rao, S. A., Weng, H. Y., & Yamagata, T. (2007). El Niño Modoki and its possible teleconnection. *Journal of Geophysical Research*, *112*, C11007. https://doi.org/10.1029/2006JC003798

Balmaseda, M. A., Mogensen, K., & Weaver, A. T. (2013). Evaluation of the ECMWF ocean reanalysis system ORAS4. *Quarterly Journal of the Royal Meteorological Society*, *139*(674), 1132–1161. https://doi.org/10.1002/qj.2063

Bejarano, L., & Jin, F.-F. (2008). Coexistence of equatorial coupled modes of ENSO. *Journal of Climate*, *21*(12), 3051–3067. https://doi.org/10.1175/2007JCLI1679.1

Bjerknes, J. (1969). Atmospheric teleconnections from the equatorial Pacific. *Monthly Weather Review*, *97*(3), 163–172. https://doi.org/10.1175/1520-0493(1969)097,0163:ATFTEP.2.3.CO;2

Bosc, C., & Delcroix, T. (2008). Observed equatorial Rossby waves and ENSO-related warm water volume changes in the equatorial Pacific Ocean. *Journal of Geophysical Research*, *113*, C06003. https://doi.org/10.1029/2007JC004613

Bunge, L., & Clarke, A. J. (2014). On the warm water volume and its changing relationship with ENSO. *Journal of Physical Oceanography*, *44*(5), 1372–1385. https://doi.org/10.1175/JPO-D-13-062.1

Cane, M. A., & Zebiak, S. E. (1985). A theory for El Niño and the Southern Oscillation. *Science*, *228*(4703), 1085–1087. https://doi.org/10.1126/science.228.4703.1085

Clark, A. J. (2010). Analytical theory for the quasi-steady and low frequency equatorial ocean response to wind forcing: The "tilt" and "warm water volume" modes. *Journal of Physical Oceanography*, *40*(1), 121–137. https://doi.org/10.1175/2009JPO4263.1

Fedorov, A. V. (2010). Ocean response to wind variations, warm water volume, and simple models of ENSO in the low frequency approximation. *Journal of Climate*, *23*(14), 3855–3873. https://doi.org/10.1175/2010JCLI3044.1

Hendon, H. H., Lim, E., Wang, G., Alves, O., & Hudson, D. (2009). Prospects for predicting two flavors of El Niño. *Geophysical Research Letters*, *36*, L19713. https://doi.org/10.1029/2009GL040100

Horii, T., Ueki, I., & Hanawa, K. (2012). Breakdown of ENSO predictors in the 2000s: Decadal changes of recharge/discharge-SST phase relation and atmospheric intraseasonal forcing. *Geophysical Research Letters*, *39*, L10707. https://doi.org/10.1029/2012GL051740

Huang, B., Thorne, M. P., Banzon, F. V., Boyer, T., Chepurin, G., Lawrimore, J. H., et al. (2017). Extended Reconstructed Sea Surface Temperature, Version 5 (ERSSTv5): Upgrades, validations, and intercomparisons. *Journal of Climate*, *30*(20), 8179–8205. https://doi.org/10.1175/JCLI-D-16-0836.1

Izumo, T., Lengaigne, M., Vialard, J., Suresh, I., & Planton, Y. (2019). On the physical interpretation of the lead relation between the warm water volume and the El Niño Southern Oscillation. *Climate Dynamics*, *52*(5-6), 2923–2942. https://doi.org/10.1007/s00382-018-4313-1

Jin, F.-F. (1997). An equatorial ocean recharge paradigm for ENSO. Part I: Conceptual model. *Journal of the Atmospheric Sciences*, *54*(7), 811–829. https://doi.org/10.1175/1520-0469(1997)054%3C0811:AEORPF%3E2.0.CO;2

Kao, H. Y., & Yu, J. Y. (2009). Contrasting eastern-Pacific and central-Pacific types of ENSO. *Journal of Climate*, *22*(3), 615–632. https://doi.org/10.1175/2008JCLI2309.1

Kug, J.-S., Jin, F.-F., & An, S.-I. (2009). Two types of El Niño events: Cold tongue El Niño and warm pool El Niño. *Journal of Climate*, *22*(6), 1499–1515. https://doi.org/10.1175/2008JCLI2624.1

McPhaden, M. J. (2003). Tropical Pacific Ocean heat content variations and ENSO persistence barriers. *Geophysical Research Letters*, *30*(9), 1480. https://doi.org/10.1029/2003GL016872

McPhaden, M. J. (2012). A 21st century shift in the relationship between ENSO SST and warm water volume anomalies. *Geophysical Research Letters*, *39*, L09706. https://doi.org/10.1029/2012GL051826

McPhaden, M. J., Zebiak, S. E., & Glantz, M. H. (2006). ENSO as an integrating concept in Earth science. *Science*, *314*(5806), 1740–1745. https://doi.org/10.1126/science.1132588

Meinen, C. S., & McPhaden, M. J. (2000). Observations of warm water volume changes in the equatorial Pacific and their relationship to El Niño and La Niña. *Journal of Climate*, *13*(20), 3551–3559. https://doi.org/10.1175/1520-0442(2000)013%3C3551:OOWWVC%3E2.0.CO;2

Neelin, J. D., Battisti, D. S., Hirst, A. C., Jin, F.-F., Wakata, Y., Yamagata, T., & Zebiak, S. E. (1998). ENSO theory. *Journal of Geophysical Research*, *103*, 14,261–14,290. https://doi.org/10.1029/97JC03424

Neske, S., & McGregor, S. (2018). Understanding the warm water volume precursor of ENSO events and its interdecadal variation. *Geophysical Research Letters*, *45*, 1577–1585. https://doi.org/10.1002/2017GL076439

Planton, Y., Vialard, J., Guilyardi, E., Lengaigne, M., & Izumo, T. (2018). Western Pacific oceanic heat content: A better predictor of La Niña than of El Niño. *Geophysical Research Letters*, *45*, 9824–9833. https://doi.org/10.1029/2018GL079341

Ren, H.-L., & Jin, F.-F. (2011). Niño indices for two types of ENSO. *Geophysical Research Letters*, *38*, L04704. https://doi.org/10.1029/2010GL046031

Ren, H.-L., & Jin, F.-F. (2013). Recharge oscillator mechanisms in two types of ENSO. *Journal of Climate*, *26*(17), 6506–6523. https://doi.org/10.1175/JCLI-D-12-00601.1

Shinoda, T., Hurlburt, H. E., & Metzger, E. J. (2011). Anomalous tropical ocean circulation associated with La Niña Modoki. *Journal of Geophysical Research*, *116*, C12001. https://doi.org/10.1029/2011JC007304

Timmermann, A., An, S.-I., Kug, J.-S., Jin, F. F., Cai, W., Capotondi, A., et al. (2018). El Niño-Southern Oscillation complexity. *Nature*, *26*, 535–545.

Wallace, J. M., Rasmusson, E. M., Mitchell, T. P., Kousky, V. E., Sarachik, E. S., & von Storch, H. (1998). On the structure and evolution of ENSO related climate variability in the tropical Pacific: Lessons from TOGA. *Journal of Geophysical Research*, *103*(C7), 14241–14259. https://doi.org/10.1029/97JC02905

Wang, W., Chen, M., & Kumar, A. (2010). An assessment of the CFS real time seasonal forecasts. *Weather and Forecasting*, *25*(3), 950–969. https://doi.org/10.1175/2010WAF2222345.1

Wyrtki, K. (1975). El Niño—The dynamic response of the equatorial Pacific Ocean to atmospheric forcing. *Journal of Physical Oceanography*, *5*(4), 572–584. https://doi.org/10.1175/1520-0485(1975)005,0572:ENTDRO.2.0.CO;2

Wyrtki, K. (1985). Water displacements in the pacific and the genesis of El Niño cycles. *Journal of Geophysical Research*, *90*(C4), 7129–7132. https://doi.org/10.1029/JC090iC04p07129

Xie, R., & Jin, F.-F. (2018). Two leading ENSO modes and El Niño types in the Zebiak-Cane model. *Journal of Climate*, *31*(5), 1943–1962. https://doi.org/10.1175/JCLI-D-17-0469.1

Zebiak, S. E. (1989). Oceanic heat content variability and El Niño cycles. *Journal of Physical Oceanography*, *19*(4), 475–486. https://doi.org/10.1175/1520-0485(1989)019,0475:OHCVAE.2.0.CO;2

Zhang, W., Jin, F.-F., & Turner, A. (2014). Increasing autumn drought over southern China associated with ENSO regime shift. *Geophysical Research Letters*, *41*, 4020–4026. https://doi.org/10.1002/2014GL060130

Zhang, W., Wang, L., Xiang, B., Qi, L., & He, J. (2015). Impacts of two types of La Niña on the NAO during boreal winter. *Climate Dynamics*, *44*(5-6), 1351–1366. https://doi.org/10.1007/s00382-014-2155-z